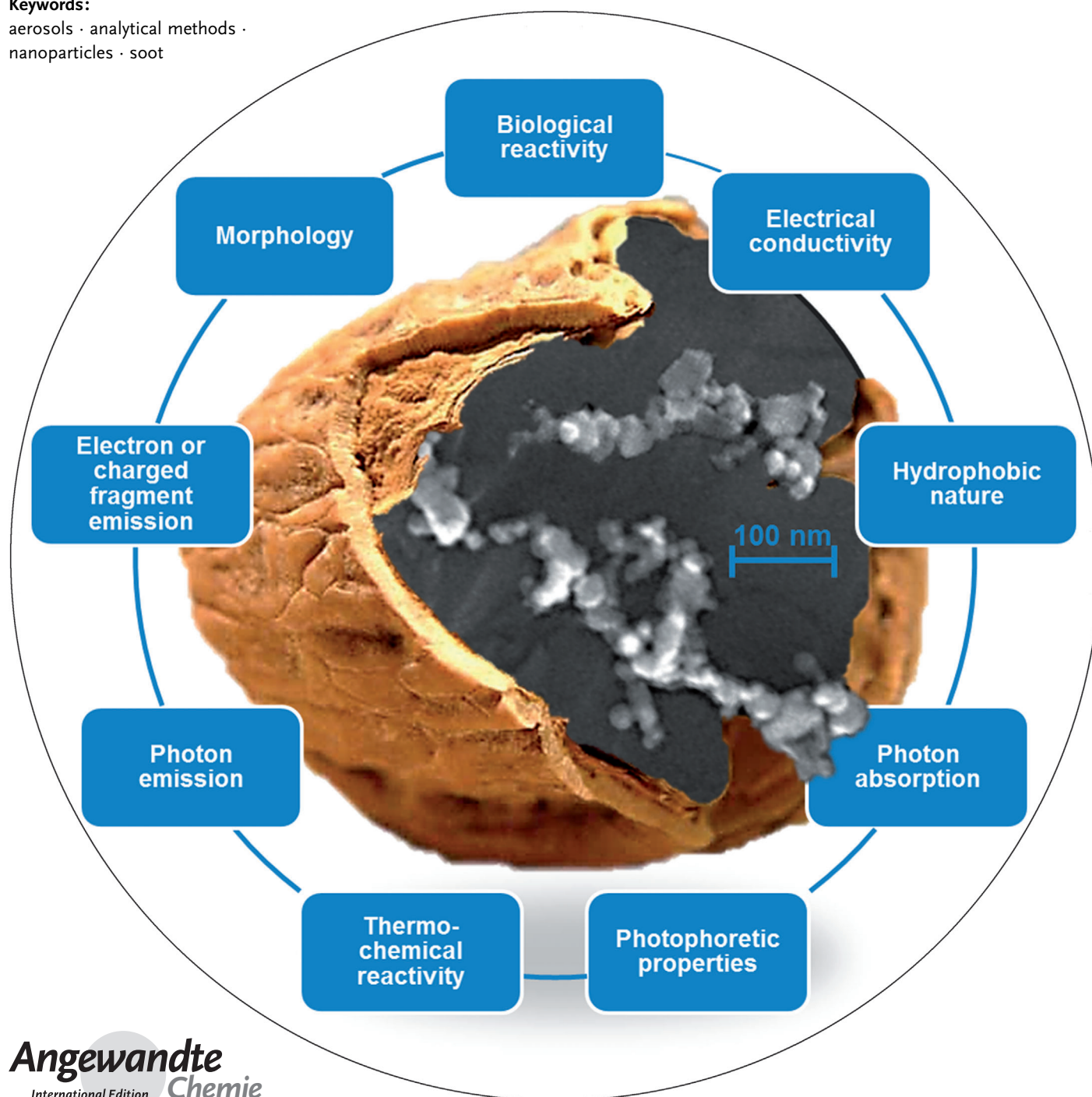# The Many Faces of Soot: Characterization of Soot Nanoparticles Produced by Engines

Reinhard Niessner*

Soot nanoparticles produced by engines constitute a threat to human health. For the analytical chemist, soot is a hard nut to crack as the released particles undergo rapid changes in their size, shape, and number concentration. The complete characterization of soot will be essential to meet future low-emission standards. Besides measuring the light extinction, modern analytical chemistry can determine a variety of less-known effects, such as condensation properties, immune response in vertebrates, and impact on the cardiovascular function of a beating heart. Photon emission and in particular Raman spectroscopy provides information on the nanocrystallinity, while thermoelectron emission allows the number of electrical particles to be counted. Even the "simple" combustion of soot nanoparticles offers potential for the characterization of the particles.

From the Contents

1. Introduction

Soot nanoparticles (NPs) produced by engines have a considerable impact on our daily life. This is connected with the increasing number of cars with combustion engines that enable mobility, flexibility, and fast logistics. Modern society expects unlimited mobility, but this is obtained with increased risks for human health.[1,2] Furthermore, air traffic and shipping is steadily increasing.

Transport powered by combustion engines cannot be replaced completely within the next few decades. Combustion engines form the basis of a functioning fast, unrestricted, and flexible transport system. For more than 100 years, we have seen a continuous development in combustion engines, fueled by either gasoline or diesel. Despite the enormous effort made in developing electromobility, the predominance of combustion engines will remain for the next 50 years. Attending conferences on automotive engineering nowadays is a real eye-opener: the very limited electric storage capacity (allowing a driving range < 250 km) and the decreasing storage capacity with falling temperatures, because of, amongst other things, the use of cabin heating during winter time, highlights the current limitation. Modern diesel-fueled engines have a better fuel efficiency than any other engines, except gas-driven engines.

Common to these engines is the unavoidable production of ultrafine particles, mainly as a result of incomplete combustion. Diesel fuel is introduced as fine droplets into the combustion chamber and incomplete combustion occurs particularly in the oxygen-deficient regions inside the droplet and in the immediate surroundings of the droplet, which mainly consists of diesel fuel vapor. Soot particles then form from the generated precursor molecules such as acetylene, nucleation, particle growth by reaction with gaseous components, coagulation, carbonization, and (partial) oxidation.[3–5] Despite continuous optimization, any combustion engine concept has to live with inhomogeneous combustion conditions in the internal combustion chamber. High-pressure injection an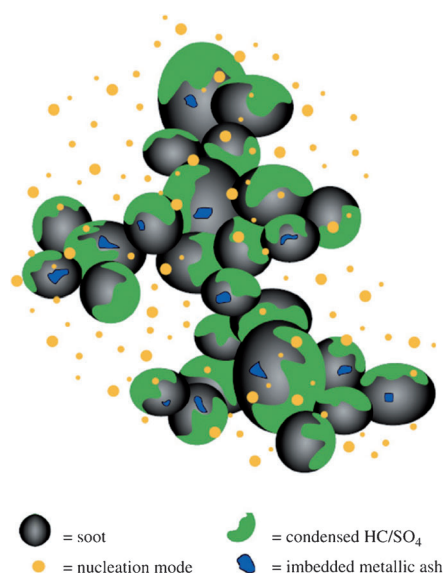d similar means provide ultrafine fuel droplets, but the combustion becomes quenched near the cylinder wall, thereby resulting in the release of either soot particles and/or noncombustible contaminants (e.g. metal oxides). Thus, depending on the combustion conditions, fuel, and lubricant composition, the emitted exhaust contains particles of complex composition: soot particles can be internally or externally mixed with minerals and coated with adsorbed semi-volatile compounds or sulfuric acid.[6,7] A typical example of NPs released from a diesel engine is shown in Figure 1.[8]

A few decades ago, typical diesel exhaust could be both smelt and seen. This is no longer the case today. Studies have shown its impact, and exhaust standards (e.g. as a result of EU regulation) now warrant a comparatively clean exhaust gas. Thus, the most modern passenger cars and the latest truck engine technologies only cause acceptable levels of pollution to the ambient air. But why is engine-released soot still a topic?

[*] Prof. Dr. R. Niessner
Institute of Hydrochemistry, Chair of Analytical Chemistry
Technische Universität München (Germany)
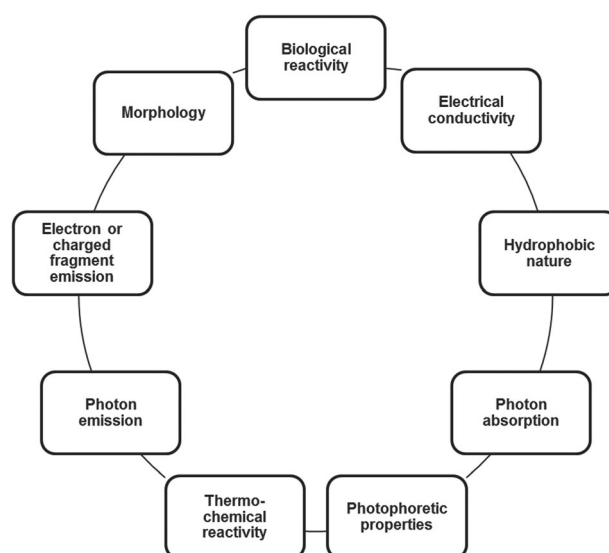E-mail: reinhard.niessner@ch.tum.de

Figure 1. An artist's view of diesel particulate matter. From Ref. [8]. Copyright 2007 Elsevier.

Figure 2. "Soot" characterization: In what connection? An Overview.

The vision of the engineers over the next few years is zero-emission engines (disregarding CO_2 emission).[9] This seems viable, if not only could the combustion be further optimized, but the so-called after-treatment (means to remove residual exhaust particles and harmful gaseous components) also actually removed the remaining aerosol particles.[10–12] Such after-treatment usually contains a diesel oxidation catalyst that oxidizes gaseous exhaust components (e.g. hydrocarbons (HCs), CO, and NO_x) to CO_2 and NO_2 and partially oxidizes soot. Secondly, most of the soot mass is trapped in a diesel particulate filter (DPF), which needs to be regenerated by actively (periodically) or passively (continuously) oxidizing the trapped soot by means of O_2 and NO_2. There are several strategies to enhance the reactivity of the soot oxidation (e.g. fuel-borne catalysts or catalyst coating on a filter substrate) so as to enhance the efficiency of DPF performance. Finally, NO_x emissions are reduced by a NO_x storage catalyst or by selective catalytic reduction (SCR). New legislation (Euro 5b/V and Euro 6/VI) limits the release of NPs to less than 6×10^{11} particles per kilometer.[13–17] In terms of mass concentration, the limits are $5\ \mathrm{mg\,km^{-1}}$ for passenger cars,

and $10\ \mathrm{mg\,kWh^{-1}}$ for trucks. The gas phase of engine exhaust is already successfully treated by different catalyst technologies.

Air traffic is also improving in terms of NP reduction, since the direct injection of particles into the stratosphere gives rise to concerns with respect to climate change.[18] Marine traffic is also under discussion. Huge engines, fired with heavy fuel oil, generate extremely complex soot NPs that are full of heavy metals and other residues from the distillation processes.[19, 20]

In the following, the focus is set on carbonaceous particles formed under a combustion scenario that is typical for passenger vehicles, trucks, as well as ships. Also included are those NPs produced under similar conditions (e.g. flame-derived or produced by plasma ignition and sparking). Beginning with the current understanding of the impact of such soot particles on human health, we will discuss the current difficulties in characterizing soot.

Soot consists of a conglomerate of carbon-containing compounds in the form of agglomerated nanoparticles. Many attempts have been reported over the last century to understand its main properties. For analysts, it is still a hard nut to crack.

To approach such a comprehensive description it is necessary to consider the extraordinary interaction of soot nanoparticles with living organisms, surrounding media (gases and liquids), and electromagnetic radiation as well as morphological visual inspection (Figure 2 and Table 1).

2. Morphological Characterization of Soot NPs by HRTEM (Size and Shape)

Numerous publications report on the morphological properties of soot aerosols produced by engines.[21–23] Since, the collected soot particles may undergo a physicochemical transition during sample preparation, depending on the engine operation, a certain, but unknown, change in the

Reinhard Niessner studied chemistry at the University of Freiburg 1976, and obtained his PhD from the University of Dortmund in 1981, where he habilitated in 1985. From 1986 to 1989 he was a Professor for Inorganic & Analytical Chemistry in Dortmund. He then became Full Professor for Analytical Chemistry at the TU Munich. His awards include the Emanuel-Merck-Prize for Analytical Chemistry (1990), the Smoluchowski-Award for Aerosol Research (1991), the Fritz-Pregl-Medal of the Austrian Society for Analytical Chemistry (1996), and the Fresenius-Award for Analytical Chemistry of the German Chemical Society (2000).

Table 1: Comprehensive characterization of soot.

Information	Method	Characteristics
morphology (size, shape) and nanostructure	HRTEM	offline; morphology and nanostructure determine the oxidation reactivity of soot[25]
biological reactivity	Langendorff heart	injected NPs lead to increased heart rate and arrythmia through release of stress hormones[1]
hydrophobic nature of carbon NPs	supersaturation in multistep condensation-nuclei counter	surface-sensitive tool for characterization of gas-suspended NPs; nucleation properties observable when NPs are introduced into the condensing system[33–35]
electrical conductivity	sensor chip with interdigital electrode structure	electrical conductivity differs by four orders of magnitude depending on soot production conditions; under development for on-board diagnosis of exhaust after-treatment functionality[36, 39–41]
light absorption		
light extinction, soot volume fraction	intracavity laser light absorption	in situ measurement of light extinction; dependent on particle size, shape, and refractive index[46–48]
particle number concentration, photon absorption (without scattering)	photoacoustic spectroscopy	fast in situ detection, data useful for engine development and climate research[49–55]
radical centers of soot particles	electron paramagnetic resonance (EPR)	offline; enables investigation of direct oxidative interaction of soot NPs with other (bi)radical molecules (e.g. NO_2 or O_2) present in combustion engine exhausts[56–58]
photophoresis		
photophoretic velocity	photophoresis	in situ description of light-absorbing properties depending on particle size, shape, refraction index, and extinction coefficient[61, 62]
soot oxidation reactivity	temperature-programmed oxidation (TPO)	TPO mimics exhaust after-treatment, soot reactivity essential for regeneration of diesel particulate filters, dependent on soot microstructure and mixed-mineral ash; offline[67–69]
photon emission		
particle mass concentration	laser-induced incandescence	high time resolution[71–74]
soot particle mass concentration	single-particle soot photometer (SP2)	for characterization of combustion emissions and for climate research[75]
defects in soot microstructure	Raman spectroscopy	soot microstructure can be correlated with soot oxidation reactivity, dispersive character of characteristic soot D-band in Raman spectrum useful[68, 76–79]
electron emission or charged carbon fragmentation		
elemental species composition	photoelectron spectroscopy (PES)	surface-sensitive analysis of bulk material[23, 80, 81]
particle number concentration	charging of NPs by excitation of thermo- or photoelectrons	online, PAH molecules on particle surface enhance sensitivity[82–86]
particle number concentration	charging of NPs by thermoelectron emission due to multiphoton absorption of visible light	potential for online counting of soot particles in exhaust[87]
composition of soot particles	aerosol mass spectrometry or ICP-MS	online single-particle analysis feasible

particle size and shape can be assumed. It is well known from chemical analysis that, depending on the fuel and lubricant composition, up to 1/3 of the aerosol mass is volatilized during the pumping-down cycle in a TEM system.[24] Nevertheless, HRTEM gives reliable information on the size and shape of soot particles. As can be seen from Figure 1, soot consists of many agglomerated nanoparticles, whose primary particle diameters are in the range of 5 to 30 nm. Single agglomerates may reach an average length in the micrometer range.

HRTEM also provides an insight into the nanostructure of soot particles. Figure 3 shows how the structure of a typical diesel engine soot lies between the two cornerstones of the nanocrystalline order of carbon particles: graphitic order and completely distorted graphene layers of spark-discharge carbon NPs.[25] The latter is of specific interest: the disordered crystallinity is responsible for its enormous reactivity towards oxidation.
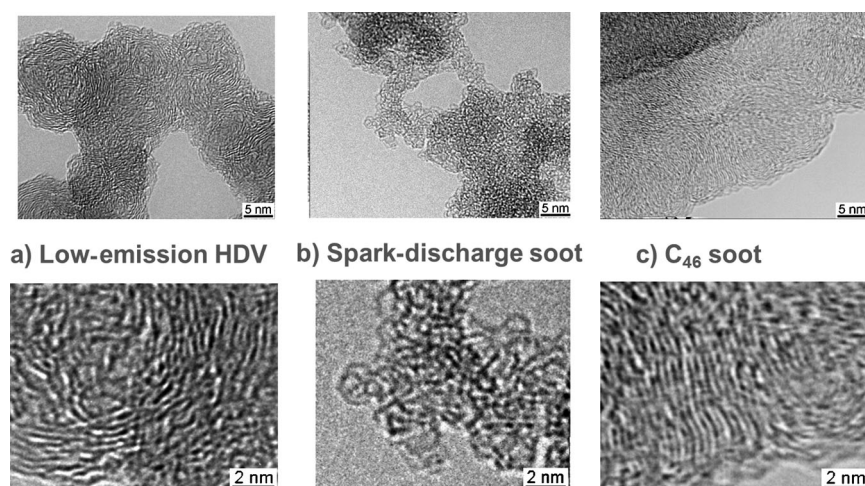
Engine soot has a nanocrystalline structure which can cover the full range between graphite and distorted carbon lattices. The pronounced differences between soot species has enormous consequences for their chemical reactivity, and this is what the after-treatment technology is dependent upon at the moment.[26–28] Only those soot species which can be combusted at low temperatures are wanted. A high reactivity of the produced soot is of utmost importance for optimizing the fuel consumption of combustion engines. Structural and chemical information on the soot NPs produced is required so that optimal burn-off conditions can be applied in the after-treatment.
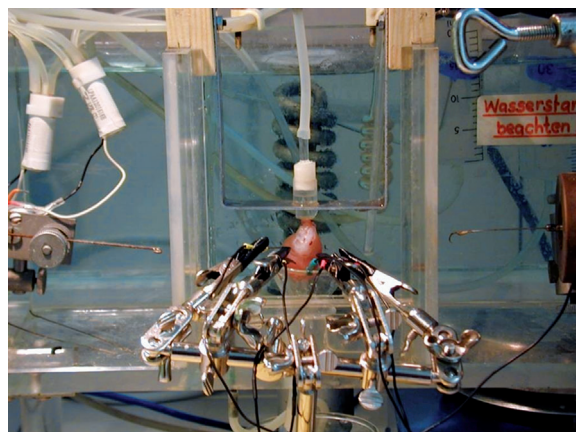
3. Biological Reactivity of Soot NPs

As early as 1775, Percival Pott identifed the detrimental effect of soot, namely for inducing scrotal cancer.[29] Aside from the usual impact of soot NPs on human health through the interaction of attached mutagenic and carcinogenic compounds,[30] soot and even pure carbon NPs show some
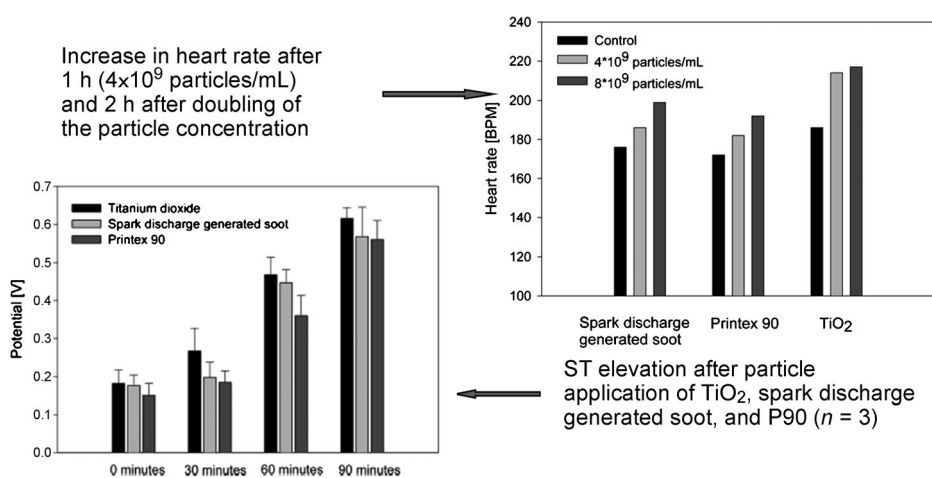
Figure 3. HRTEM micrographs of Euro IV soot from a low-emission engine (a), spark-discharge soot (b), and hexabenzocoronene as a graphite model compound (c). From Ref. [25]. Copyright 2004 Elsevier.

peculiar health effects. Since the end of the last century we also know more about the ability of soot to be an immune system responder. It was shown in an immunization experiment that rabbits respond to soot nanoparticles in a similar way as to protein-bound polycyclic aromatic hydrocarbons (PAHs).[31] Usually a PAH molecule (as a small antigen) itself is not able to produce highly affine IgG class antibodies. Since the soot NPs used in these experiments were created by the degradation of acetylene by a laser plasma, only the graphitic parts of the individual NPs could serve as a trigger of the PAH-structure-recognizing IgG populations present in the vertebrates. It would be interesting to see whether immunization with other carbon NPs would yield differently selective antibodies.

An even more interesting approach to assess the health effect of soot NPs is not to use individual tests with different endpoints, but to use an intact heart.

Stampfl et al. published experiments with an excised guinea pig heart[1] (the so-called Langendorff heart; Figure 4). They added NP dispersions into the blood stream of a still beating heart and observed its response by electrocardiography. Besides SiO_2 and TiO_2 NPs, engineered carbon NPs were also applied. Carbon NPs of various origin were found to increase the heart beat rate (Figure 5) and also evoked arrhythmia.

The reason for this was the release of catecholamines, which were also found in the circulating blood serum by a separately conducted LC/MS analysis. The additional supply of a β-blocker immediately suppressed this effect. Unpublished work with this Langendorff heart arrangement revealed considerable differences in response, for example, when testing single-wall and multiwall carbon nanotubes.

Figure 4. Langendorff heart apparatus as a test model for bioresponse to "soot". From Ref. [1]. Copyright 2011 American Chemical Society.

From what is known so far, carbon NPs trigger the immune system and affect the cardiovascular performance directly through interaction with internal cell surfaces. This may be strongly influenced by the hydrophobic nature and shape of the individual particles. Unfortunately, a systematic study with well-defined carbon-particle systems has not yet been performed.

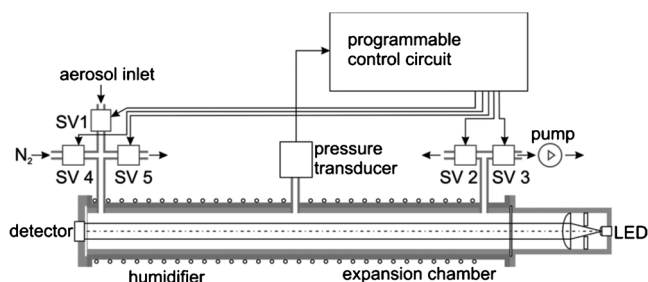Further studies on the cytotoxicity and inflammatory potential of soot particles interestingly reveal that, at the same mass concentration, soot particles generated under low-emission conditions in accordance with the regulations of Euro IV possess

Figure 5. Cardiovascular effects after the injection of soot, TiO_2, or Printex 90, as measured by ECG. From Ref. [1]. Copyright 2011 American Chemical Society.

a much higher toxic and inflammatory potential than soot particles generated with an old diesel engine working under black-smoke conditions.[32] The authors of the study assign this effect to the enhancement of defects in the structure of the Euro IV soot compared to soot released by the old engine.
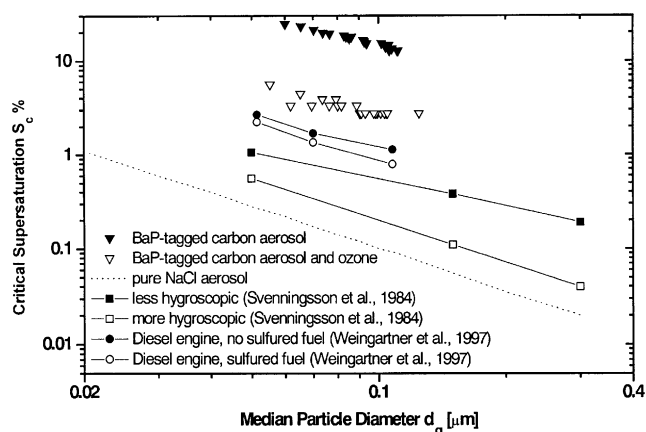
4. Probing the Hydrophobic Nature of Carbon NPs

From the above discussion, the characterization of the hydrophobicity/hydrophilicity of soot or carbon NPs seems to be of crucial importance. However, such measurement is not trivial, since it has to be performed in situ. Unbiased observation of the behavior of an individual particle is only possible within an aerosol where it is in a dispersed state. Fortunately, aerosol science offers some tools for this kind of analysis that are applicable to soot aerosols. Water condensation on a particle is determined by the particle size, surface composition, and local water supersaturation. Therefore, we have to initiate water condensation on a monodisperse soot aerosol as condensation nuclei. As long as the particles are of the same size, only the formation of drops from condensing water molecules (when hitting a particle surface under supersaturation conditions) can prove the wettability. Under such conditions, the water supersaturation required for droplet formation reflects the hydrophobic character of a carbon particle surface. Figure 6 shows the experimental setup used for such experiments.[33–35]

The monodisperse soot sample, classified by means of a continuous differential mobility analyzer, is introduced into the chamber of a condensation-nuclei counter. Its wall is permanently wetted by water and kept at a constant temperature, thereby establishing 100% relative humidity. After a short equilibration time of a few seconds, particle-free gas is injected into the aerosol sample within the condensation chamber. The pressure is then increased up to a predetermined overpressure by a computer-driven programme. A residence time of a few seconds again allows for equilibration of the humidity. In a next step, the two solenoid valves at the ends of the chamber are opened within 15 ms, thereby creating an adiabatic water supersaturation of up to several hundred percent. Depending on the size and wettability (expressed by the contact angle for the formation of a water droplet on the surface of the soot particle), supersaturation occurs, where transmitted light becomes attenuated by the extinction of the formed droplets.

Figure 6. Condensation-nuclei counter with variable water supersaturation. From Ref. [35]. Copyright 2010 Springer.
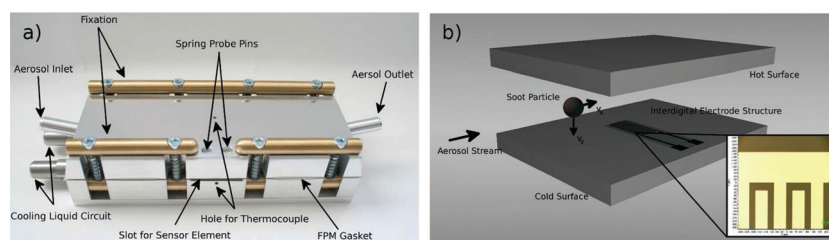

Figure 7. Critical supersaturations for spark-discharge soot aerosols and for real aerosols measured by other authors as a function of particle diameter. From Ref. [34]. Copyright 1999 Pergamon.

Figure 7 shows the condensation properties of different soot NP systems. As can be seen, soot consisting of BaP-tagged spark-discharge carbon is extremely hydrophobic, especially compared to NaCl- and H_2SO_4-contaminated aerosols. In the case of combustion aerosols, sulfur-containing fuel leads to H_2SO_4 patches on the carbon surfaces, which has the consequence that lower water supersaturation is needed to trigger condensation. Gas/particle reactions, for example, between ozone and particles, can result in a drastic change in the surface properties. The formation of hydroxy groups on the NP surface (verified by NIR reflectance spectroscopy) results in a high hydrophilicity. This was proved by the following multistep condensation: the reaction of soot NPs with 1 ppmv ozone in air leads to a shift of more than 20% in the water supersaturation to smaller values within a reaction time of 120 s.

It can be concluded that heterogeneous water nucleation can be used as a surface-sensitive tool for characterizing gas-suspended nanoparticles. It delivers no direct chemical information, but reflects the mechanism whereby NPs become incorporated into a condensing system (e.g. during cloud or fog formation).

5. Soot Characterization by Conductivity Measurements

Soot particles, which consist mainly of carbon, can show a considerable electrical conductivity. This is well known in the case of graphite particles. A different situation exists for typical exhaust agglomerates. Soot produced by diesel engines contains up to 20 wt% of inorganic compounds, depending on the fuel quality, additives, and lubricant composition. Conductance measurements on such aerosols can be performed by directly depositing them on a typical interdigital resistivity sensor chip.[36] A highly efficient way of obtaining a representative sample size that is independently and homogeneously distributed across the sensor structure is through the use of a thermophoretic NP sampler. Figure 8 shows such a sampling system. It consists of two parallel plates
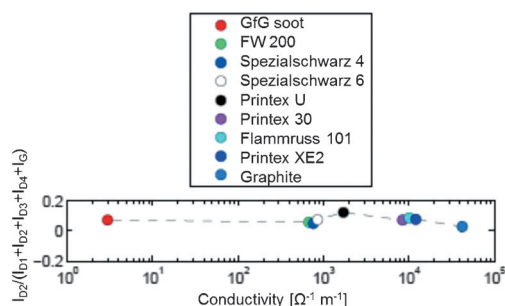
Figure 8. Thermophoretic precipitator with a cooled and heated plate (a) and a slot for a conductometric soot sensor with interdigital electrodes (b). From Ref. [36]. Copyright 2012 American Chemical Society.

with a 450-µm spacing between, one heated and the other cooled. The temperature gradient of up to 140 K leads to gas collisions that results in a net force which directs the nanoparticles in a size-independent manner[37] to the cold wall, where the conductometric sensor element is embedded.

The DC resistivity of soot powder (Figure 9) has been measured by a Van der Pauw arrangement.[38] We found differences of four orders of magnitude in the conductivity of differently produced soot in this experiment under identical conditions (p, T). The nanocrystallinity of the soot NPs again determines this behavior: Only in the case of well-ordered and symmetrical unit cells (as with graphitic particles) is a high conductivity obtained. In the case of a distorted structure, as is found for the spark-discharge carbon NPs, the particles are nonconductive. As the content of the non-conductive inorganic material incorporated into a soot agglomerate is increased, the conductivity diminishes.

This behavior has practical consequences: so-called on-board diagnosis of small and larger engine-driven vehicles is currently being carried out. In the future, the regulation asks for a permanent monitoring of the function of the after-treatment system. The first prototypes, based on such resistivity sensors, are under study.[39–41] The exhaust aerosol becomes deposited onto an interdigital electrode sensor positioned behind the diesel particulate filter of the after-treatment system and the conductance is continuously measured on board. The more soot per unit of time that becomes deposited, the less the after-treatment is working. Detailed studies have shown that chemical transition of deposited soot, for example, by reaction with NO_2 at temper-

atures around 700 K, occurs and also changes the specific conductivity.

It seems that conductivity measurements on NP deposits may be a convenient substitute for expensive quantitative analysis tools.

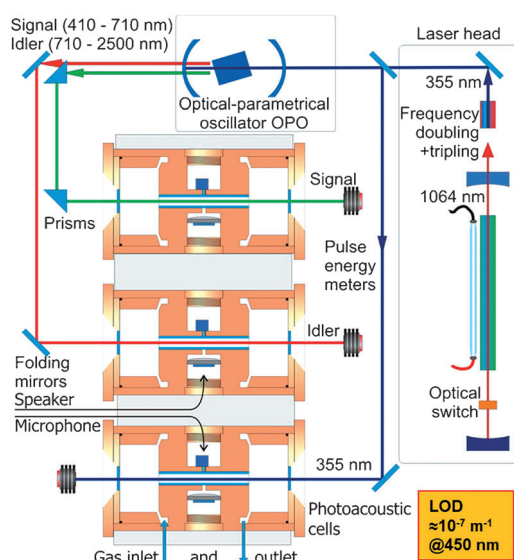## 6. Soot Characterization by Interaction with Electromagnetic Radiation: Photon Absorption

Soot NPs consist mainly of carbon in different forms (such as graphite, fullerene etc.), but an admixture with other contaminants is also frequently observed.[42,43] For example, metal oxides are often mixed into soot particles. In aerosol science this is termed an internally mixed soot particle. The electromagnetic behavior of such soot NPs is greatly affected by the distribution of inorganic matter inside or at the particle surface. A black carbon particle can be twinned with a transparent inorganic particle or the carbon covers an iron oxide core. Soot can have a black or brownish appearance, or something in between, because of the presence of other carbon forms (e.g. fullerene).[44]

Fresh combustion aerosols undergo fast agglomeration through Brownian motion. The application of in situ techniques is a must for the analysis of such an unstable NP system with particle sizes of a few nanometers.

Since soot is an efficient absorber of light, one would think first of using light attenuation for in situ characterization. Light absorption, mainly as an extinction-based technique, is frequently used for the detection of soot aerosols.[45] Intracavity absorption of laser light by aerosol particles leads to a dramatic reduction of the emitted laser light, and could be used in principle for the in situ extinction measurement.[46] Only one application on re-dispersed graphene oxide aerosol has been reported to date. However, all extinction-based techniques (e.g. light transmission) also depend on the size, shape, and refractive index of the particle.[47,48] Techniques that yield information on true absorption properties are today preferred.

The classical method to observe these absorption properties is photoacoustic spectroscopy, where optical energy absorbed by a particulate analyte is converted into heat. As a consequence of the local warming of a light-absorbing particle system, the surrounding gas phase is heated and expands. There are several ways to measure this expansion, and in most applications open acoustic resonators that are continuously filled with the NP aerosol are illuminated by a modulated laser beam.[49–54] Depending on the geometry of the acoustic resonator, when at its resonance frequency the absorbed energy leads to various pressure modes within the tube which are detected by small electret microphones placed near the local pressure maximum. Hence, not only does the power of the irradiating light source determine (together with the light-absorption properties of the dispersed NPs) the detection limit, but the geometry of the acoustic resonator has an enormous effect on the amplitude of a generated pressure

Figure 9. DC conductivity of "soot" powder measured by a Van der Pauw arrangement. Conditions described in Ref. [36].
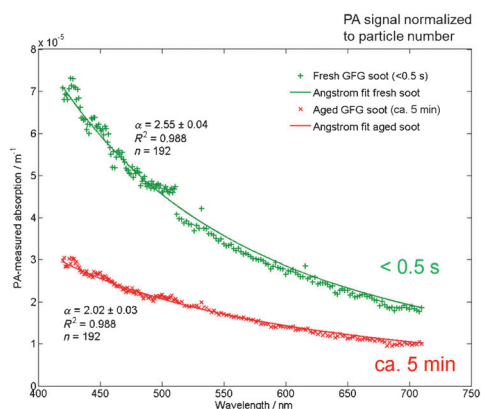
Figure 10. Layout of the pulsed photoacoustic aerosol absorption spectrometer. The spectrometer features a spectral range of 410 to 2500 nm and a sensitivity of 2.5×10^{-7} m^{-1} at 550 nm. From Ref. [55]. Copyright 2012 American Chemical Society.

wave. Since the laser power and the resonator geometry are constant, the measured pressure signal is directly proportional to the mass of the irradiated carbon particle.

Figure 10 shows the latest set up of a laser-based aerosol absorption spectrometer.[55] An OPO laser system is used, which covers a wavelength range of 410 to 2500 nm. The pulsed laser beam passes various serially arranged photoacoustic cells. Filtered and unfiltered aerosol samples are analyzed separately so that the light absorbed by the carrier gas can be subtracted. Figure 11 depicts the absorption properties of differently aged soot aerosols.

As can be seen, an increase in light absorption is only observed at the energy-rich part of the spectrum because of

Figure 11. Absorption spectra of fresh and aged spark-discharge soot measured with the photoacoustic absorption spectrometer. The corresponding absorption curves between 410 and 710 nm are shown. The Ångström coefficients given in the following are calculated by fitting the equation to the measured data, based on the wavelength range from 410 to 700 nm and a wavelength step of 2 nm. From Ref. [55]. Copyright 2012 American Chemical Society.

agglomeration. No distinct spectral features can be detected. The true absorption coefficient can be measured by photoacoustic spectroscopy. These data are needed not only by the engineers developing the engines as a tool for inspecting a running engine under fast changing operations, but these data are also needed in climate research to calculate the radiation budget for sunlight radiation illuminating the global atmosphere. The Ångstrom coefficient expresses the spectral dependence of the optical thickness of the soot aerosol.

It is also possible to characterize soot NPs with low energy electromagnetic radiation, namely by using radio frequencies in the 10-GHz range. Since soot has an enormous number of unpaired electrons, the application of electron paramagnetic resonance (EPR) spectroscopy is extremely promising.[56–58] A newly born particle is incomplete in terms of C−C bond formation. The spark-discharge soot exhibits the highest electron spin densities of up to 10^{-5} per carbon atom. This stems from the extreme temperature gradient during sparking between graphite electrodes. Typical diesel soot has a ten times lower spin density. EPR allows the direct oxidative interaction of other (bi)radical molecules (e.g. NO_2 or O_2) with soot particle surfaces to be probed, which is the key step in after-treatment technology.

Unfortunately, this promising technique is only applicable in a batch mode, which requires the sampling of several milligrams of soot.
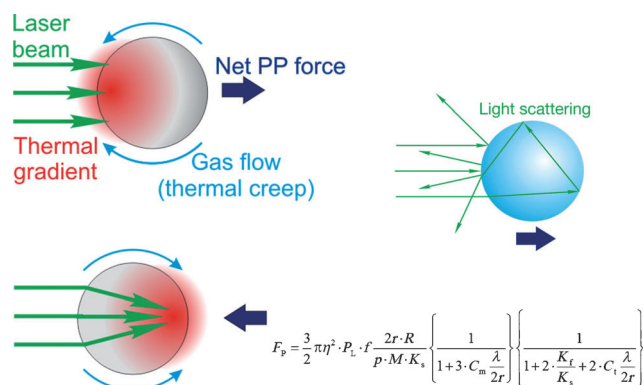
7. Characterization of Soot NPs by Photophoresis

As mentioned in the previous section, interaction with photons may lead to the warming of soot NPs, and the consequential gas expansion can be used to determine the photon absorption properties. However, photons do not only transfer energy to the appropriate absorbing particles, they are also able to move a particle through inhomogeneous heating. This effect, called photophoresis, was first detected in 1917 by Ehrenhaft.[59] Physicists have observed the movement of small dispersed aerosol particles when exposed to a photon flux from a strong light source. These particles showed irregular movements, differing in the direction of travel and the speed.[60] Nowadays, the advent of laser sources and particle tracking allows the photophoretic behavior to be used to classify NP systems.
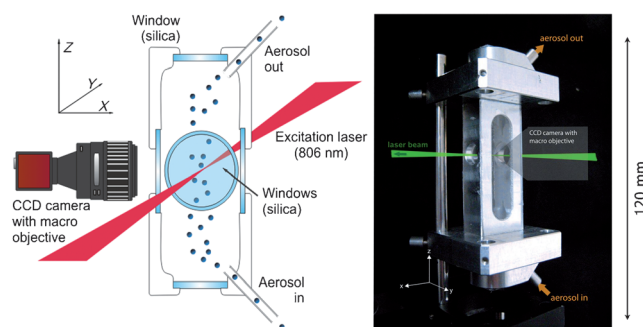
In photophoresis (the principle is shown in Figure 12), the particle under illumination may respond in different ways. The photophoretic velocity will depend on the optical properties—which can be rather complex—the particle size, and the properties of the gas.

In the case of a particle that partially absorbs inhomogeneously, the intrinsic properties of the NP absorption govern the traveling direction. If the light is absorbed at the illuminated front part of the NP, a net force occurs as a result of gas molecules creeping around the NP, which moves the particle away. In the case of semitransparent particles, the heating up occurs at the opposite non-illuminated face of the particle, with the consequence of a net force towards the light source. Each particle system is characterized by its intrinsic specific photophoretic velocity.

$$F_p = \frac{3}{2}\pi\eta^2 \cdot P_L \cdot f \frac{2r \cdot R}{p \cdot M \cdot K_s} \left\{ \frac{1}{1+3 \cdot C_m \frac{\lambda}{2r}} \right\} \left\{ \frac{1}{1+2 \cdot \frac{K_t}{K_s} + 2 \cdot C_t \frac{\lambda}{2r}} \right\}$$

Figure 12. Aerosol photophoresis of differently absorbing nanoparticles. Positive and negative photophoresis is caused by inhomogeneous photon absorption. A thermo-photophoretic force arises when uneven heating of the particle leads to temperature differences in the surrounding gas. Molecules of the heated gas in proximity to hot particle regions start to impinge on the surface with higher kinetic energy than molecules in proximity to cold surface regions, thereby resulting in a net force on the particle contrary to the temperature gradient.
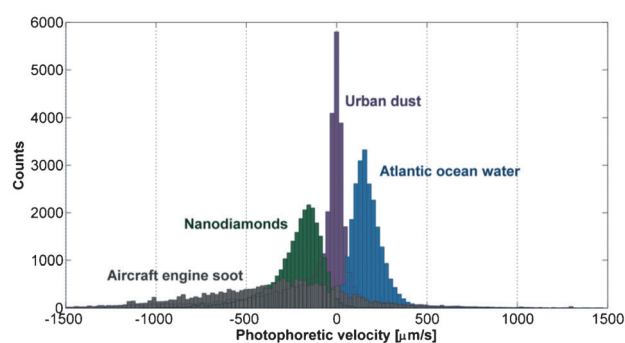

Figure 13. Experimental setup for determining the photophoretic particle velocity (schematic drawing and photograph). From Ref. [61]. Copyright 2008 American Chemical Society.
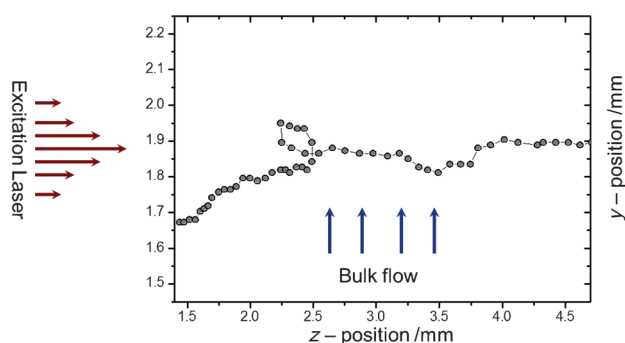

Figure 14. Photophoretic velocity of soot and nanodiamonds in comparison to resuspended urban dust and sea spray. From Ref. [62]. Copyright 2010 IOP Publishing.

Figure 15. The uncommon photophoretic behavior of soot agglomerates. Shown is the trajectory of one spark-discharge soot particle ($d_p \approx 200$ nm).

Figure 13 shows a typical experimental arrangement used for photophoresis.[61] A small optically accessible aerosol chamber, continuously flooded with the aerosol under study, is illuminated by a strong (1 W) continuous wave NIR laser (806 nm). Perpendicular to this, a green laser visualizes the aerosol by light scattering. The interaction volume is observed by a CCD camera with a macro objective. The individual particle trajectories are viewed by continuous particle tracking, and the particle velocities can be calculated.

The first experiments with different aerosols including soot revealed interesting features (Figure 14): steady-state particle velocities and directions could be identified that depended on the optical properties of the spray-generated particles.[62] Deeply colored NPs migrate with high velocity (μm s^{-1}) towards the laser source. Nanodiamonds and sea spray showed movement away from the light source. Figure 15 depicts the unusual (and so far theoretically unresolved) behavior of agglomerated freshly prepared spark-discharge soot.

This soot type not only shows the highest particle velocity, it also shows irregular movements, even with changing directions and loops when entering the laser beam. It might be expected that this irregular movement is caused when only a part of such an agglomerate becomes heated up.

Currently, there is no other tool known for such an in situ description of light-absorbing NPs, either singly dispersed or agglomerated. This behavior may further become exploited for an optical, continuous particle separation. First attempts of this have been reported.

8. Characterization of Soot Reactivity by Temperature-Programmed Oxidation (TPO)

The attempted generation of particle-free diesel engine exhaust by means of an after-treatment is usually performed by continuous particle filtration.[63] There are two widely used approaches: one uses dead-end filtration with porous honeycomb ceramic structures, which necessitates the regular burn off of the sampled soot. The second application is the use of half-open filter units, where most of the particles become deposited. In both cases, oxygen or nitrogen dioxide (the latter artificially increased in concentration) are the oxidants for soot removal.[64–66] Not only does the increased back pressure across a plugged filter unit increase the overall fuel (energy) consumption, the frequent burn-off is also unwanted due to the additional fuel consumption for DPF regeneration.

To meet the requirement of an easy to perform (in the sense of being low energy) burn-off, the reactivity of the soot NPs systems have to be determined by temperature-programmed oxidation. For such a thermoanalytical approach, metallic fiber filters are used to collect soot NPs in a first step. This soot-loaded filter is then incorporated in a programmable heater unit (Figure 16): the combustion typically is intended to mimic the conditions in the after-treatment section: 5 vol% O_2, 95 vol% N_2 in a temperature range of 300 to 1100 K.[67]
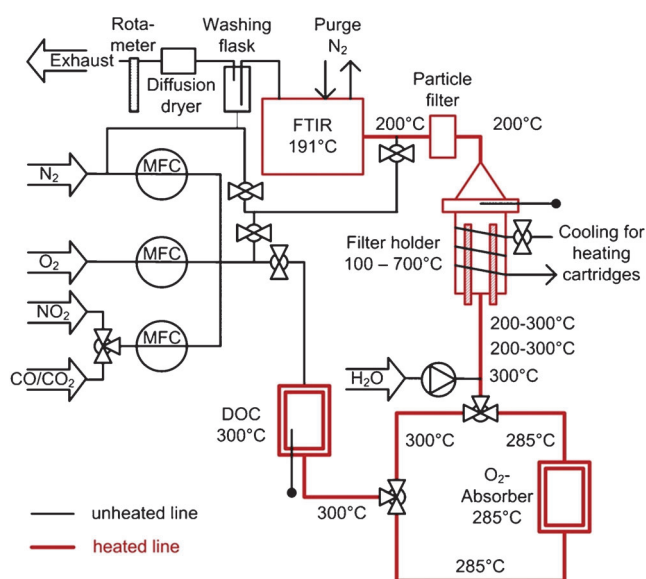
Under these conditions, soot combusts to CO_2 and CO. Figure 17 shows the result of the analysis of a 10 mg sample of soot.[68]

It becomes apparent that "soot" is not simply "soot": graphite is by far the most inert and stable (up to 1100 K) carbon form, while spark-discharge soot already becomes partly oxidized at around 500 K because of its completely distorted nanocrystallinity. Typical diesel NPs show oxidation reactivity in between these two carbon forms. Currently, engine developers are trying to find engine operation conditions where the soot produced shows a low-temperature combustion similar to spark-discharge soot. As described above, this would also mean a non-negligible cost-saving potential.
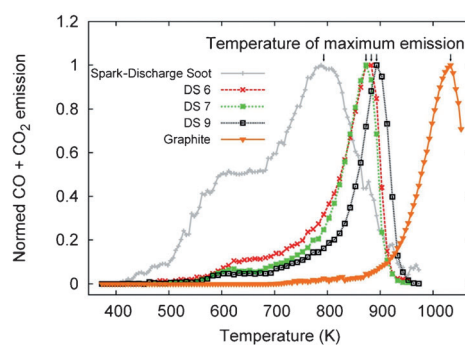
Over the last few decades, many attempts have been made to influence the combustion reactivity by forming admixtures with additives such as CeO_2, iron compounds, and others. Figure 18 depicts the results of a recent study, where iron-doped soot NPs were produced by adding $Fe(CO)_5$ to a propane flame, operated under oxygen-deficient conditions.[69]

It is clearly seen in the TPO measurement that the increasing percentage of Fe to C results in a dramatically diminished temperature onset of soot combustion.

In a further study we could show that alkali or alkaline earth salt additives show a comparable effect. It seems that in the case of Fe additives, a certain part of the reactivity is
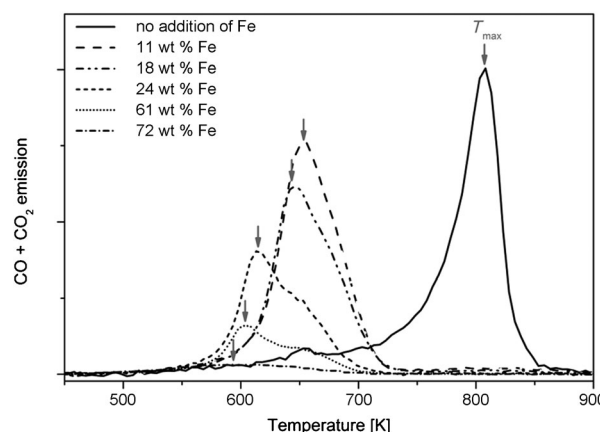

$$RI_{Soot} = 100 \left(\frac{T_{Soot} - T_{Graphite}}{T_{GfG} - T_{Graphite}} \right)$$

Reactivity limits:
spark-discharge soot
= 100%;
graphite = 0%

Figure 17. Oxidation behavior of soot with increasing temperature described by a) the emission of oxidation products and b) mass conversion of three diesel soot samples and controls (spark discharge soot and graphite). From Ref. [68]. Copyright 2011 American Chemical Society.

Figure 18. TPO analysis of $Fe(CO_5)$-doped flame-derived "soot". TPO profiles for six propane soot types of different Fe content normalized to the soot mass on the filter. Arrows indicate the maximum total emission temperatures T_{max}. From Ref. [69]. Copyright 2012 Taylor and Francis.

explained by the oxygen-donor properties of the iron oxide which is included in the soot NP structure. In the case of non-oxygen-containing salts, the inclusion or intercalation of alkali metals between the graphene layers disturbs the symmetry and opens the way for an oxidative attack.

Car manufacturers would appreciate having an online version of TPO, since the current practice has a low throughput (1 sample/2 h).

9. Characterization of Soot NPs by Photon Emission

Photon emission is a pillar of analytical spectroscopy. The question is, though, whether soot particles can be made

Figure 16. Temperature-programmed oxidation under simulated exhaust conditions.

luminescent. The presence of conjugated double bonds and other structural elements, together with satisfying the necessary selection rules, are responsible for the selective luminescence of organic compounds.
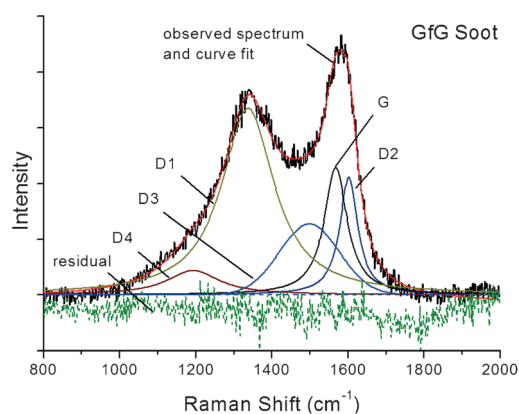
It has been known for 20 years that the application of laser fluorescence as an in situ tool for surface-enriched soot NPs does not lead to convincing results. Even strongly fluorescing PAHs do not exhibit fluorescence when adsorbed in sub-monolayers on soot NPs.[70] Clearly, either the strong sorption changes the structural geometry of attached PAH molecules or a nonradiative energy transfer to the soot particle core occurs.

Since soot NPs are good light absorbers, experiments with pulsed laser light were soon applied after its introduction in the 1970s. Nanosecond laser illumination heats soot NPs up to approximately 4000 K by multiphoton absorption. Such hot particles lose at least part of their stored energy by black body radiation: they start glowing. Hot soot NPs can be observed through this, and a quantitative measurement of the mass concentration is feasible by integrating the light emitted after excitation with a laser pulse.[71–74] The advantage of this in situ characterization is the high time resolution, only limited by the repetition rate of the laser pulse. Sensitivities down to a few ng C m^{-3} have been reported. Attempts have also been made to determine the individual particle size by analyzing the time decay of the incandescence of singly observed NPs.

A similar approach is realized in the single-particle soot photometer (SP2). The most advanced version uses an Nd-YAG laser (1064 nm) and two avalanche photodetectors to observe the inelastic scattering produced inside the laser cavity under fixed observation angles. Soot NPs in the upper nanometer size range exhibit light scattering and incandescence in parallel because of the strong photon flux.[75]

A completely different situation (in terms of specifity) is found when a laser stimulates Raman emission. Pronounced G- and D-band Raman emission, which reflects the nanocrystalline order within a soot NP, was already found in the 1970s.[76] Figure 19 shows these remarkable Raman features of soot.
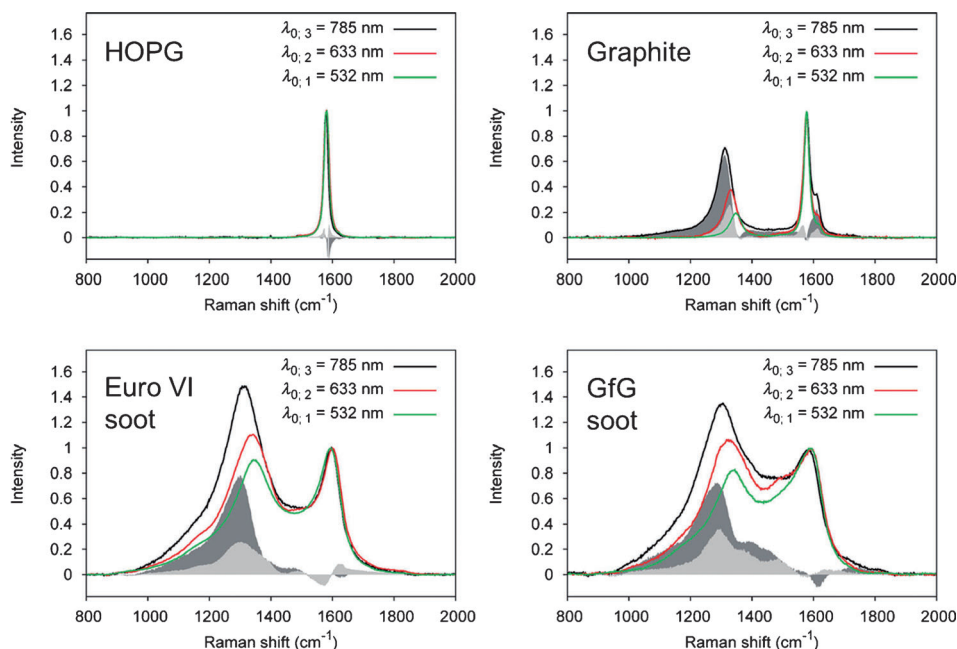
Highly oriented graphite (only consisting of sp^2 bonds with perfect nanocrystallinity) shows a rather narrow band, the so-called G (graphite) peak.[77] Once this ability to form a perfect lattice is prevented by combustion or other non-optimal conditions, a second peak, the D (distorted) peak evolves. Furthermore, the classic rule of the absorption wavelength invariance of the

Figure 19. Raman microspectroscopy of spark-discharge soot showing the presence of graphite-like crystalline domains and amorphous domains. Particle size is 10–30 nm ($\lambda_0 =$ at 514 nm).
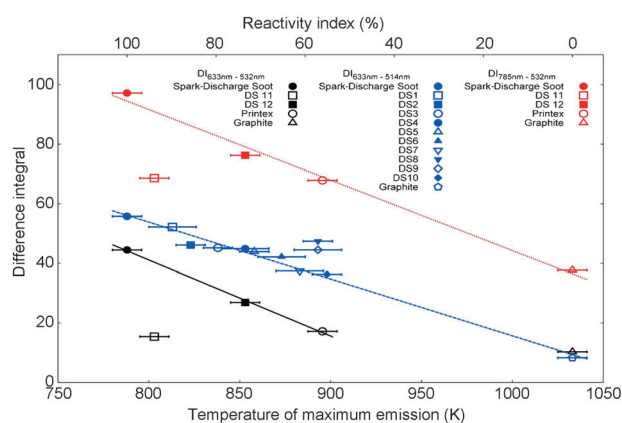
Raman shift is not valid for such soot NPs because of the broken symmetry in a double phonon effect.[68] Only the perfect symmetry (nanocrystallinity) within a highly oriented pyrolytic graphite (HOPG) sample shows the absorption wavelength invariance when irradiated under different laser excitation wavelengths (Figure 20). If applied to typical soot NPs or to spark-discharge soot, the broken symmetry leads to pronounced changes in the D-band as a function of the applied excitation wavelength. A good correlation is found between these findings and the corresponding TPO results (Figure 21).

Nowadays, we apply Raman spectroscopy, either applied at one excitation wavelength and using the ratio of the G- and

Figure 20. Raman spectra of a) HOPG, b) graphite powder, c) diesel soot 12 (Euro IV), and d) spark-discharge soot (sorted by increasing structural disorder) measured at different excitation wavelengths ($\lambda_{0;1} = 532$ nm, $\lambda_{0;2} = 633$ nm, $\lambda_{0;3} = 785$ nm). The dark gray areas are the result of the subtraction of the $\lambda_{0;1}$ spectra from the $\lambda_{0;3}$ spectra, and the light gray areas from the subtraction of the $\lambda_{0;1}$ spectra from the $\lambda_{0;2}$ spectra. From Ref. [68]. Copyright 2011 American Chemical Society.

Figure 21. Correlation of the TPO results (maximum emission temperature) versus difference integral of the Raman emission at different excitation wavelengths. The reactivity index range spans from spark-discharge soot to graphite. From Ref. [68]. Copyright 2011 American Chemical Society.

D-peak intensities and band width to describe soot NPs, or we analyze soot at different wavelengths and use the integrated peak area to describe the reactivity of the soot to oxidation. As long as no other activator, as for example a metal salt or oxide additives, are present, this approach is a valid tool for predicting soot oxidation.[78,79]

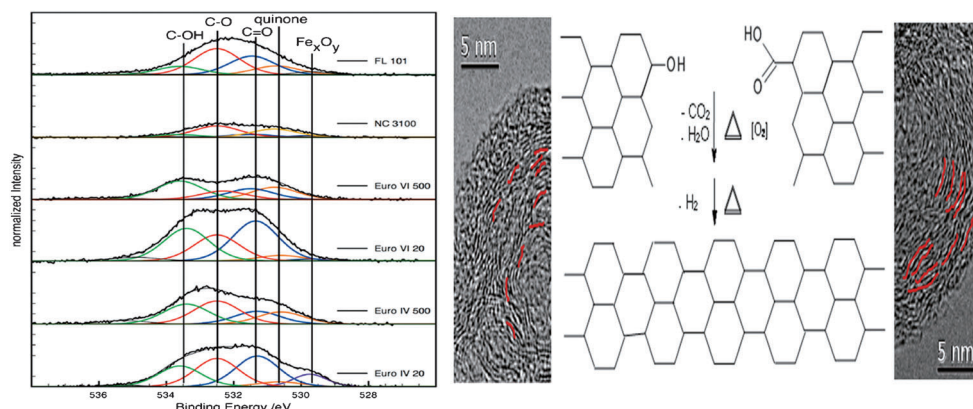## 10. Characterization of Soot NPs by Electron Emission or Charged Carbon Fragmentation

The emission of electrons from soot NPs can be stimulated in different ways. The classical application is photoelectron spectroscopy (PES).[23,80] The use of a monochromatic X-ray source (usually $Mg_{K\alpha}$ or $Al_{K\alpha}$ radiation) allows the kinetic energy of the released photoelectrons to be measured and allows calculation of the binding energy. This is a well-accepted approach in surface science, but also reveals the limitation of this tool for bulk analysis of aerosol particles. Only those elements which undergo a substantial chemical shift depending on the electronic situation of the respective element will give a hint to the chemical structure and oxidation state. Unfortunately, carbon does not show a strong chemical shift. Soot modifications and the chemical structure of a soot NP, therefore, cannot be easily resolved. Furthermore, photoelectrons only become released from the outer parts of a soot NP because of the extreme surface sensitivity. Thus, it only probes the surface. If one is interested in the change in the surface chemistry under, for example, thermal stress, as with TPO, then PES is a rather sensitive tool.[81] Figure 22 shows the change in the reactivity of a typical diesel exhaust soot to oxygen. As can be seen from the combined application of HRTEM and PES, the thermal treatment leads to the formation of new carbon–carbon bonds and loss of CO_2/CO. These results were confirmed by TPO experiments.

A different measurement principle is the excitation of thermo- or photoelectrons, which leaves positively charged soot NPs. The charging of suspended soot particles by pulsed light sources was known from early studies, carried out 100 years ago.[82] Millikan already used this working principle to obtain charged particles in his famous experimental setup. It took about 70 years until UV light was applied for the online detection of soot aerosols, mainly from diesel engine combustion.[83–85] Further experiments using laser-excited photoelectron emission under ambient pressure showed the crucial role of attached large PAH molecules as "antenna pigments". The larger the adsorbed PAH molecules are, the lower is the energy threshold limit for photoelectron emission. The relation of the applied laser energy to charges generated at a fixed wavelength confirmed a single-photon excitation.[86]

In the case when visible light was used, which is clearly below the threshold limit for carbon photoelectron emission, a multiphoton absorption and the release of thermoelectrons was observed at an increased laser fluence (up to $50 \, \text{mJ cm}^{-2}$).[87] This could be used for the online counting of soot particles. The in situ charged NPs are continuously measured by filtration inside a Faraday cup. This approach is now under study again, since the new PMP regulation asks for particle concentrations to be measured instead of the soot mass concentration.

Finally, the application of a laser to vaporize soot particles inside the ionizer chamber of an aerosol mass spectrometer and measurement of the produced carbon ions has been reported.[88] The use of an inductively coupled plasma mass spectrometer (ICP-MS) for the online analysis of single carbon particles also seems feasible.[89]

Figure 22. O1s X-ray photoelectron spectroscopy applied to different soot species (Flammruss 101, NC 3100, GfG, Euro IV, and Euro VI diesel soot) under oxidative temperature stress. The right hand side shows schematically the reordering after dehydration, which is supported by TEM curvature analysis. From Ref. [81]. Copyright 2011 American Chemical Society.

11. Conclusion

Soot released from various combustion or plasma surroundings exhibits an extremely diverse behavior when in contact with living matter or electromagnetic radiation. There is certainly no simple way to characterize soot NPs. Like all particle systems, they possess an intrinsically indefinite possibility of complexity. Only technically generated soot aerosols may have reduced variability in their internal structure and outer surface composition, as well as their size and charging state. It seems that only a combination of analytical principles yields ample information. In the case of engine-related questions, the combination of Raman spectroscopy and temperature-programmed analysis is currently used to obtain the required information. Other applications of carbon NPs, for example, as dye pigments for staining purposes, will need spectral characterization. Photoacoustic spectroscopy seems to be the method of choice, since in contrast to reflectometry (not discussed here) the size and shape has no influence.

The fast description of the contact surface properties of individual, suspended carbon NPs remains open. Further development in instrumentation is certainly needed, for example, to observe the initial contact between a cell surface and the NP itself.

Techniques which offer in situ and online observations will become of utmost importance. Soot consists of labile agglomerates of primary NPs which finally govern the optical properties and its residence time within the atmosphere once released. It is also clear that each soot NP may differ in its chemical composition within an ensemble of particles. Thus, the observation of a single particle is highly desired. Furthermore, because of the rapidly changing composition of fuel and oil over the next few years (due to the increasing amount of blended diesel or biofuel, as well as new additives), the NPs released from the chemical reactor, the "combustion engine", will undergo a steady change. 3D chemical imaging by synchrotron X-ray absorption experiments are within reach, but are still time-consuming and will remain rare.

As said at the beginning: soot has many faces and remains a hard nut to crack!

[1] A. Stampfl, M. Maier, R. Radykewicz, P. Reitmeir, M. Göttlicher, R. Niessner, *ACS Nano* **2011**, *5*, 5345–5353.
[2] B. Frank, M. Schuster, R. Schlögl, D. Su, *Angew. Chem.* **2013**, *125*, 2736–2741; *Angew. Chem. Int. Ed.* **2013**, *52*, 2673–2677.
[3] B. Stanmore, J. Brilhac, P. Gilot, *Carbon* **2001**, *39*, 2247–2268.
[4] M. Frenklach, *Phys. Chem. Chem. Phys.* **2002**, *4*, 2028–2037.
[5] J. Xi, B.-J. Zhong, *Chem. Eng. Technol.* **2006**, *29*, 665–673.
[6] H. Sakurai, H. Tobias, K. Park, D. Zarling, K. Docherty, D. Kittelson, P. McMurry, P. Ziemann, *Atmos. Environ.* **2003**, *37*, 1199–1210.
[7] J. Moldanová, E. Fridell, H. Winnes, S. Holmin-Fridell, J. Boman, A. Jedynska, V. Tishkova, B. Demirdjian, S. Joulie, H. Bladt, N. Ivleva, R. Niessner, *Atmos. Meas. Tech.* **2013**, *6*, 3577–3596.
[8] M. Maricq, *J. Aerosol Sci.* **2007**, *38*, 1079–1118.
[9] Y. Wang, C. Zhang, J. Zhang, *Adv. Mater. Res.* **2012**, *354–355*, 429–432.
[10] J. Neeft, M. Makkee, J. Moulijn, *Fuel Process. Technol.* **1996**, *47*, 1–69.
[11] T. Johnson, *Int. J. Engine Res.* **2009**, *10*, 275–285.
[12] A. Russell, W. Epling, *Catal. Rev.* **2011**, *53*, 337–423.
[13] European Parliament, Regulation (EC) No. 715/2007 of the European Parliament and of the Council of 20th June 2007 on type approval of motor vehicles with respect to emissions from light passenger and commercial vehicles (Euro 5 and Euro 6) and on access to vehicle repair and maintenance information. *Official Journal of the European Union*, **2007**.
[14] Umweltbundesamt, Abgasgrenzwerte für Lkw und Busse (Fahrzeuge ab 2610 kg, Grenzwerte für die Typ- und Serienprüfungen, **2012.**
[15] European Parliament, Regulation No. 83 of the Economic Commission for Europe of the United Nations (UN/ECE)-Uniform provisions concerning the approval of vehicles with regard to the emission of pollutants according to engine fuel requirements (Revision 3). *Official Journal of the European Union*, **2006**.
[16] European Parliament, Regulation No. 49 of the European Commission for Europe of the United Nations (UN/ECE)-Uniform provisions concerning the measures to be taken against the emission of gaseous and particulate pollutants from compression ignition engines for use in vehicles, and the emission of gaseous pollutants from positive-ignition fuelled with natural gas or liquefied petroleum gas for use in vehicles. *Official Journal of the European Union*, **2011**.
[17] B. Giechaskiel, A. Mamakos, J. Andersson, P. Dilaro, G. Martini, W. Schindler, A. Bergmann, *Aerosol Sci. Technol.* **2012**, *46*, 719–749.
[18] U. Schumann, H. Schlager, F. Arnold, J. Ovarlez, H. Kelder, O. Hov, G. Hayman, J. Isaksen, J. Staehelin, P. Whitefield, *J. Geophys. Res.* **2000**, *105*, 3605–3631.
[19] J.-M. Diesch, F. Drewnick, T. Klimach, S. Borrmann, *Atmos. Chem. Phys.* **2013**, *13*, 3603–3618.
[20] O. Popovicheva, E. Kireeva, N. Persiantseva, M. Timofeev, H. Bladt, N. Ivleva, R. Niessner, J. Moldanová, *J. Environ. Monit.* **2012**, *14*, 3101–3110.
[21] R. Vander Wal, A. Yezerets, N. Currier, D. Kim, C. Wang, *Carbon* **2007**, *45*, 70–77.
[22] M. Wentzel, H. Gorzawski, K.-H. Naumann, H. Saathoff, S. Weinbruch, *J. Aerosol Sci.* **2003**, *34*, 1347–1370.
[23] J.-O. Müller, D. Su, U. Wild, R. Schlögl, *Phys. Chem. Chem. Phys.* **2007**, *9*, 4018–4025.
[24] U. Mathis, R. Kaegli, M. Mohr, R. Zenobi, *Atmos. Environ.* **2004**, *38*, 4347–4355.
[25] D. Su, R. Jentoft, J.-O. Müller, D. Rothe, E. Jacob, K. Müllen, A. Messerer, U. Pöschl, R. Niessner, R. Schlögl, *Catal. Today* **2004**, *90*, 127–132.
[26] D. Fino, *Sci. Technol. Adv. Mater.* **2007**, *8*, 93–100.
[27] J. Adler, *Int. J. Appl. Ceram. Technol.* **2005**, *2*, 429–439.
[28] J. Yang, M. Stewart, G. Maupin, D. Herling, A. Zelenyuk, *Chem. Eng. Sci.* **2009**, *64*, 1625–1634.
[29] E. Hall, *Health Phys.* **1998**, *75*, 357–366.
[30] M. Ema, M. Naya, M. Horimoto, H. Kato, *Reprod. Toxicol.* **2013**, *42*, 1–17.

[31] D. Matschulat, H. Prestel, F. Haider, R. Niessner, D. Knopp, *J. Immunol. Methods* **2006**, *310*, 159–170.

[32] D. Su, A. Serafino, J.-O. Müller, R. Jentoft, R. Schlögl, S. Fiorito, *Environ. Sci. Technol.* **2008**, *42*, 1761–1765.

[33] R. Niessner, C. Helsper, *J. Aerosol Sci.* **1985**, *16*, 201–209.

[34] R. Kotzick, R. Niessner, *Atmos. Environ.* **1999**, *33*, 2669–2677.

[35] R. Niessner in *Nanoparticles in the Water Cycle* (Eds.: F. H. Frimmel, R. Niessner), Springer, Heidelberg, **2010**, pp. 13–21.

[36] B. Grob, J. Schmid, N. Ivleva, R. Niessner, *Anal. Chem.* **2012**, *84*, 3586–3592.

[37] A. Messerer, R. Niessner, U. Pöschl, *J. Aerosol Sci.* **2003**, *34*, 1009–1021.

[38] L. van der Pauw, *Philips Res. Rep.* **1958**, *13*, 1–9.

[39] A. Kondo, S. Yokoi, T. Sakurai, S. Nishikawa, T. Egami, M. Tokuda, T. Sakuma, *SAE Int. [Spec. Publ.]* **2011**, *2318*, 55–63.

[40] N. Li, D. Tang, C. Li, L. Chen, *Appl. Mech. Mater.* **2013**, *336–338*, 196–199.

[41] T. Ochs, H. Schittenhelm, A. Genssle, B. Kamp, *SAE Int. J. Fuels Lubr.* **2010**, *3*, 61–69.

[42] N. Nejar, J. Garcia-Cortés, C. Salinas-Martinez de Lecea, M. Illán-Gómez, *Catal. Commun.* **2005**, *6*, 263–267.

[43] R. Caprotti, I. Field, J. Michelin, S. Schuerholz, F. Terres, *Soc. Automot. Eng. [Spec. Publ.] SP* **2003**, *1802*, 105–132.

[44] G. Wolff, R. Klimisch, *Particulate Carbon Atmospheric Life Cycle*, Plenum, New York, **1982**.

[45] I. Ng, H. Ma, D. Kittelson, A. Miller, *SAE Int. [Spec. Publ.]* **2007**, *2089*, 287–294.

[46] G. Mehdi, A. Muravjov, H. Saxena, C. Fredricksen, T. Brusentsova, R. Peale, O. Edwards, *Proc. SPIE* **2011**, *8032*, 80320E/1–80320E/7.

[47] A. Petzold, C. Kopp, R. Niessner, *Atmos. Environ.* **1997**, *31*, 661–672.

[48] A. Petzold, R. Niessner, *Mikrochim. Acta* **1995**, *117*, 215–237.

[49] A. Petzold, R. Niessner, *Sens. Actuators B* **1993**, *14*, 640–641.

[50] A. Petzold, R. Niessner, *Appl. Phys. B* **1996**, *63*, 191–197.

[51] L. Krämer, Z. Bozoki, R. Niessner, *Anal. Sci.* **2001**, *17*, 563–566.

[52] H. Beck, R. Niessner, C. Haisch, *Anal. Bioanal. Chem.* **2003**, *375*, 1124–1129.

[53] W. Schindler, C. Haisch, H. Beck, R. Niessner, E. Jacob, D. Rothe, *Soc. Automot. Eng. [Spec. Publ.] SP* **2004**, *1862*, 151–158.

[54] C. Haisch, R. Niessner, *Anal. Chem.* **2012**, *84*, 7292–7296.

[55] C. Haisch, P. Menzenbach, H. Bladt, R. Niessner, *Anal. Chem.* **2012**, *84*, 8941–8945.

[56] C. Yamanaka, T. Matsuda, M. Ikeya, *Appl. Radiat. Isot.* **2005**, *62*, 307–311.

[57] S. Kamm, *Wiss. Ber.-Forschungszentrum Karlsruhe* **2000**, (FZKA6499), i-vi, 148.

[58] A. Chughtai, M. Atteya, J. Kim, B. Konowalchuk, D. Smith, *Carbon* **1998**, *36*, 1573–1589.

[59] F. Ehrenhaft, *Phys. Z.* **1917**, *18*, 352–368.

[60] O. Preining in *Aerosol Science* (Ed.: C. N. Davies), Academic Press, London **1966**, pp. 111–135.

[61] C. Haisch, C. Kykal, R. Niessner, *Anal. Chem.* **2008**, *80*, 1546–1551.

[62] C. Haisch, L. Opilik, M. Hays, R. Niessner, *J. Phys. Conf. Ser.* **2010**, *214*, 012011.

[63] W. Maus, R. Brück, F. Kaiser, *Fortschr.-Ber. VDI Reihe 12* **2002**, *490*, 175–195.

[64] A. Messerer, D. Rothe, U. Pöschl, R. Niessner, *Top. Catal.* **2004**, *30*/31, 247–250.

[65] A. Messerer, H.-J. Schmid, C. Knab, U. Pöschl, R. Niessner, *Chem. Ing. Tech.* **2004**, *76*, 1092–1096.

[66] A. Messerer, D. Rothe, R. Niessner, U. Pöschl, *Chem. Ing. Tech.* **2005**, *77*, 881–886.

[67] A. Messerer, R. Niessner, U. Pöschl, *Carbon* **2006**, *44*, 307–324.

[68] J. Schmid, B. Grob, R. Niessner, N. Ivleva, *Anal. Chem.* **2011**, *83*, 1173–1179.

[69] H. Bladt, J. Schmid, E. Kireeva, N. Persiantseva, K. Heister, M. Timofeev, J. Uihlein, O. Popovicheva, N. Ivleva, R. Niessner, *Aerosol Sci. Technol.* **2012**, *46*, 1337–1348.

[70] F. Lewitzka, R. Niessner, *Aerosol Sci. Technol.* **1995**, *23*, 454–464.

[71] C. Dasch, *Appl. Opt.* **1984**, *23*, 2209–2215.

[72] A. Eckbreth, *J. Appl. Phys.* **1977**, *48*, 4473–4479.

[73] R. L. VanderWal, *Appl. Opt.* **1996**, *35*, 6548–6559.

[74] M. Stephens, N. Turner, J. Sandberg, *Appl. Opt.* **2003**, *42*, 3726–3736.

[75] R. Gao, J. Schwarz, K. Kelly, D. Fahey, L. Watts, T. Thompson, J. Spackman, J. Slowik, E. Cross, J.-H. Han, P. Davidovits, T. Onasch, D. Worsnop, *Aerosol Sci. Technol.* **2007**, *41*, 125–135.

[76] H. Rosen, T. Novakov, *Nature* **1977**, *266*, 708–710.

[77] A. Sadezky, H. Muckenhuber, H. Grothe, R. Niessner, U. Pöschl, *Carbon* **2005**, *43*, 1731–1742.

[78] N. Ivleva, A. Messerer, X. Yang, R. Niessner, U. Pöschl, *Environ. Sci. Technol.* **2007**, *41*, 3702–3707.

[79] M. Knauer, M. Carrara, D. Rothe, R. Niessner, N. Ivleva, *Aerosol Sci. Technol.* **2009**, *43*, 1–8.

[80] R. Toossi, *Combust. Flame* **1992**, *90*, 1–10.

[81] M. Schuster, M. Hävecker, R. Arrigo, R. Blume, M. Knauer, N. Ivleva, D. Su, R. Niessner, R. Schlögl, *J. Phys. Chem. A* **2011**, *115*, 2568–2580.

[82] A. Joffe, *Sitzungsber. K. Bayerischen Akad. Wiss.* **1913**, 19–37.

[83] H. Burtscher, L. Scherrer, H. Siegmann, A. Schmidt-Ott, *J. Appl. Phys.* **1982**, *53*, 3787–3791.

[84] R. Niessner, *J. Aerosol Sci.* **1986**, *17*, 705–714.

[85] R. Niessner, B. Hemmerich, P. Wilbring, *Anal. Chem.* **1990**, *62*, 2071–2074.

[86] R. Niessner, H. Schröder, W. Robers, K. Kompa, *J. Aerosol Sci.* **1988**, *19*, 491–500.

[87] W. Robers, H. Schröder, K. Kompa, R. Niessner, *Z. Phys. Chem.* **1988**, *159*, 129–148.

[88] J. Onasch, A. Trimborn, E. Fortner, J. Jayne, G. Kok, L. Williams, P. Davidovits, D. Worsnop, *Aerosol Sci. Technol.* **2012**, *46*, 804–817.

[89] R. Reed, D. Goodwin, K. Marsh, S. Capracotta, C. Higgins, D. Fairbrother, J. Ranville, *Environ. Sci. Proc. Impacts* **2013**, *15*, 204–213.